Electronic Supplementary Material (ESI) for Journal of Materials Chemistry A.

Supporting Information

Highly efficient and green fabrication of a modified C nanofiber interlayer for high-performance Li-S batteries

Keshi Wu,[ab] Yi Hu,*[abc] Zhen Shen,[ab] Renzhong Chen,[ab] Xia He,[ab] Zhongling Cheng[ab] and Peng Pan[ab]

a. *Key Laboratory of Advanced Textile Materials and Manufacturing Technology, Ministry of Education, Zhejiang Sci-Tech University, Hangzhou, 310018, PR China*

b. Engineering Research Center for Eco-Dying & Finishing of Textiles, Ministry of Education, Zhejiang Sci-Tech University, Hangzhou, 310018, PR China

c. Dyeing and Finishing Institute of Zhejiang Sci-Tech University. Hangzhou 310018, P. R. China.

*Corresponding author. E-mail: huyi-v@zstu.edu.cn

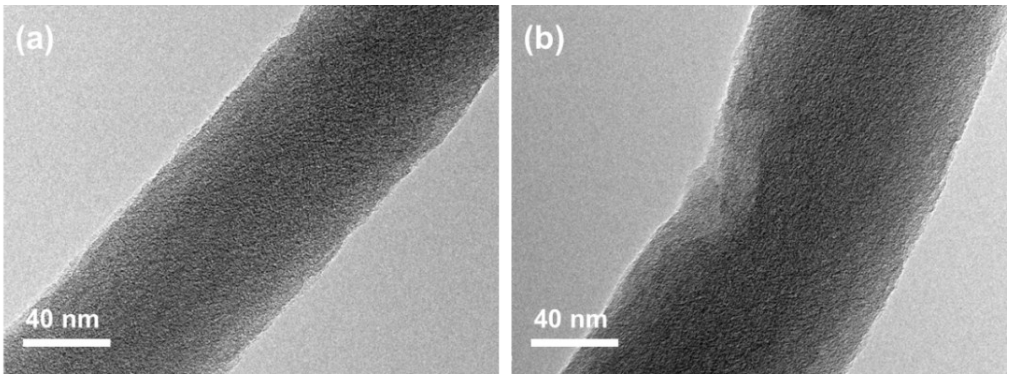

Figure S1 TEM images of (a) CNF and (b) EUV-CNF. EUV-CNFs were placed 0.5 cm away from the excimer UV lamp in air and irradiated for 20 min with 100% power.

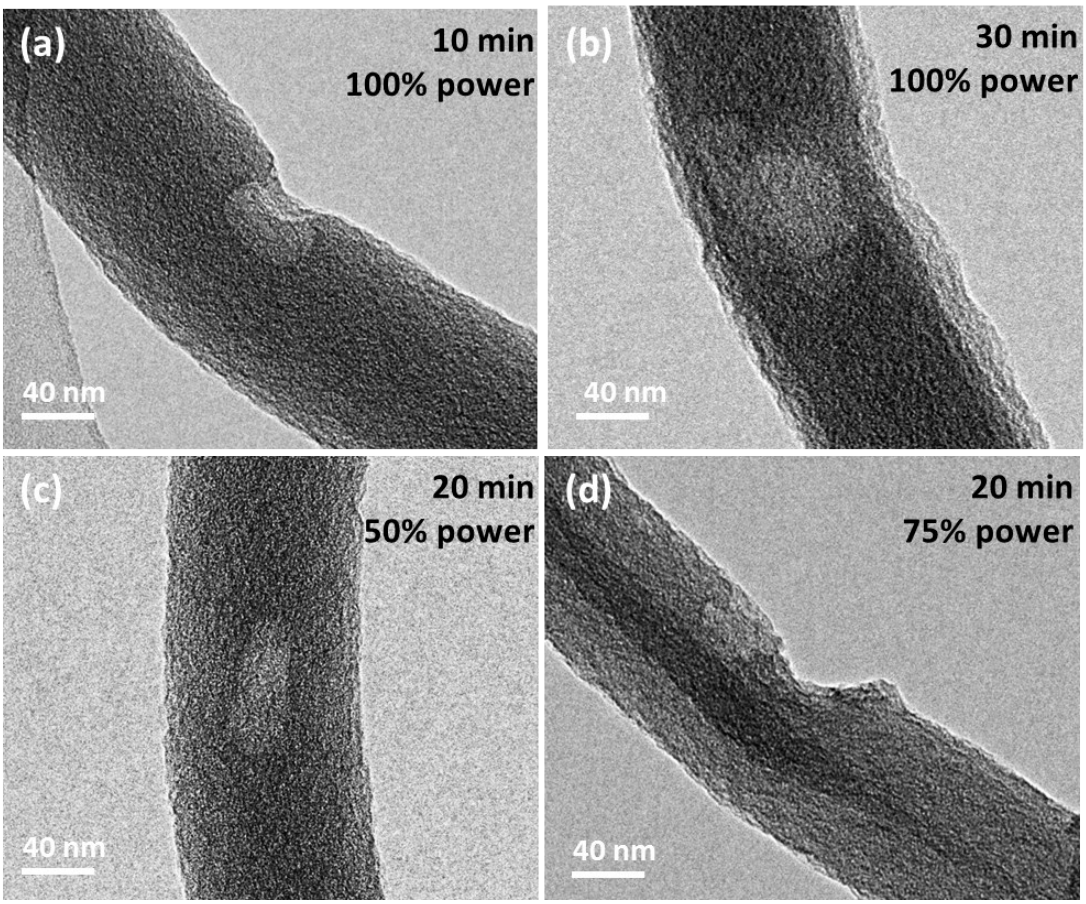

Figure S2 TEM images of EUV-CNFs irradiated for (a) 10 min at 100% power, (b) 30 min at 100% power; (c) 20 min at 50% power, (d) 20 min at 75%.

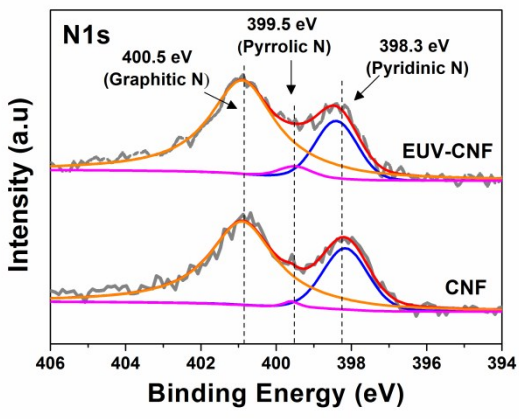

Figure S3 N 1s XPS spectra of CNF and EUV-CNF interlayers.

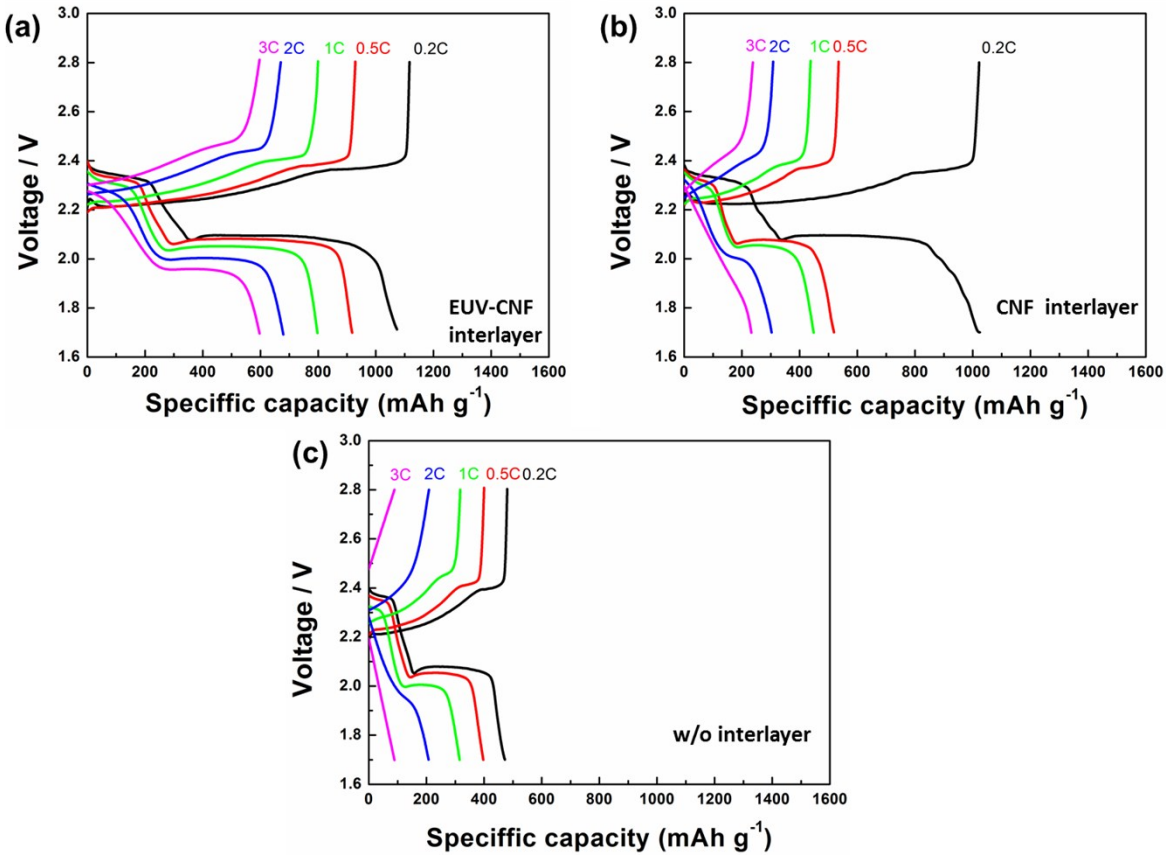

Figure S4 Discharge-charge curves recorded at 0.2, 0.5, 0.1, 2, and 3 C for Li-S batteries with (a) EUV-CNF, (b) CNF, and (c) no interlayer.

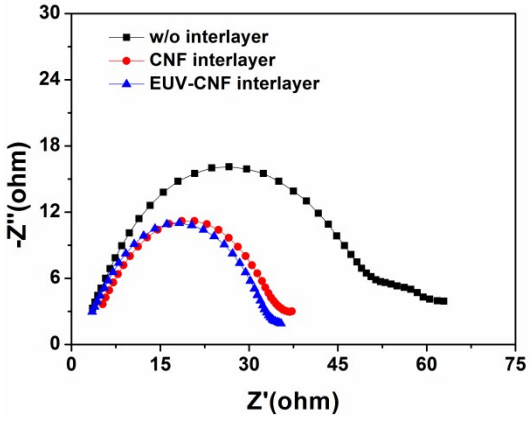

Figure S5 Nyquist plots of non-cycled Li-S batteries with EUV-CNF, CNF, and no interlayer in the frequency range of 1 MHz to 1 Hz.

Electrochemical impedance analysis was performed to compare non-cycled Li-S batteries containing EUV-CNF, CNF, and no interlayer. The diameter of the semicircle in Nyquist plots corresponded to charge transfer resistance (R_{ct}),[1,2] which equaled 31.8, 32.1, and 60.4 Ω for EUV-CNF, CNF, and interlayer-free cells, respectively. The improved reaction kinetics of the pure sulfur cathode was ascribed to the increase of its electrical conductivity after the incorporation of conductive interlayers as additional current collectors. Moreover, fresh cells with EUV-CNF and CNF interlayers showed similar R_{ct} values, indicating little change of conductivity after excimer UV light irradiation.

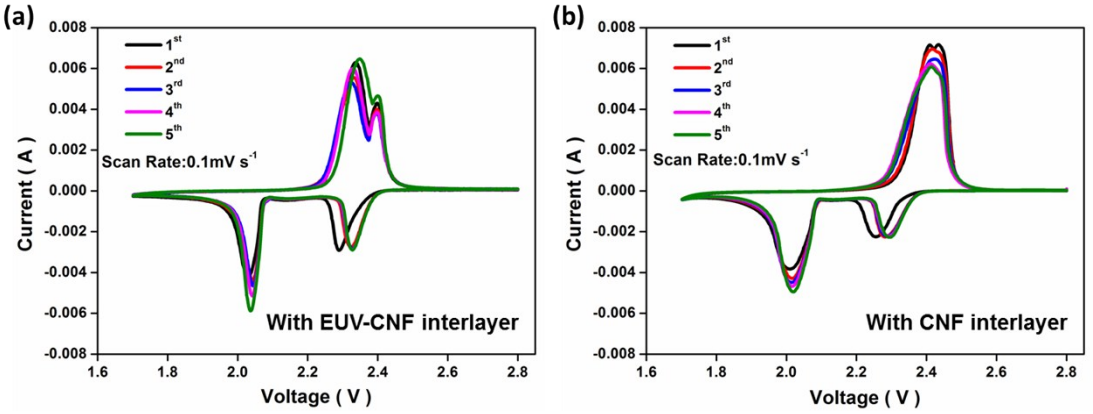

Figure S6 Cyclic voltammograms of Li-S batteries with (a) EUV-CNF interlayer and (b) CNF interlayer recorded at a scan rate of 0.1 mV s^{-1}.

CV curves of cells with EUV-CNF and CNF interlayers recorded for the first five cycles at a scan rate of 0.1 mV s^{-1} are shown in Figures S6a and b, respectively. The two main cathodic peaks at ~2.33 and 2.04 V correspond to the reduction of S_8 to Li_2S_x ($4 \le x \le 8$) and of Li_2S_4 to Li_2S_2/Li_2S, respectively. During cell charging, two continuous anodic peaks were observed at ~2.34 and 2.40 V, corresponding to the oxidation of Li_2S_2/Li_2S to Li_2S_8/S_8. Sharp peaks were observed for both EUV-CNF and CNF interlayer cells, indicating the high conductivity of both interlayers and fast electrochemical kinetics. The above cathodic and anodic peaks showed no severe potential shifts after the first cycle, which confirmed their reversibility and stability.

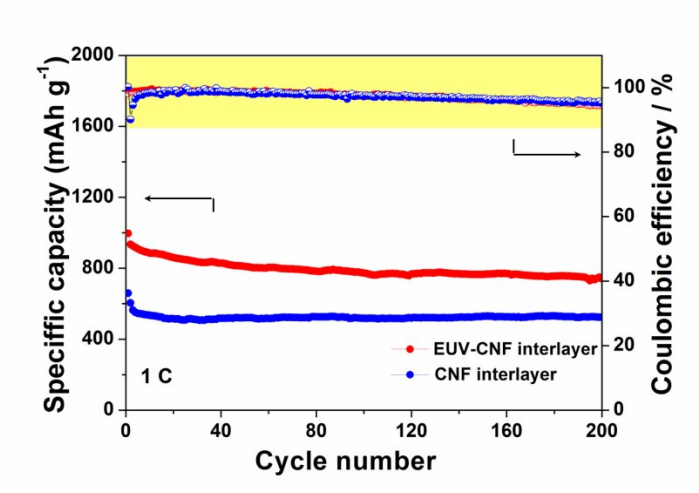

Figure S7 Discharge-charge capacities and coulombic efficiencies determined for EUV-CNF and CNF interlayer cells at a rate of 1 C over 200 cycles.

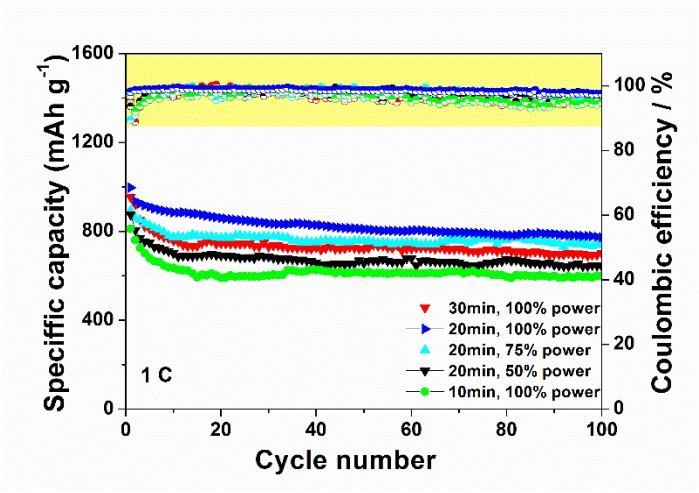

Figure S8 Discharge-charge capacities and coulombic efficiencies determined at a rate of 1 C for cells with EUV-CNF interlayers prepared under different conditions.

The cycling performances of EUV-CNF interlayers prepared under different conditions at a rate of 1 C are shown in **Figure S8**, which reveals that the discharge capacity was affected by irradiation conditions. The highest initial discharge capacity of 996 mAh g^{-1} and a high reversible capacity of 772 mAh g^{-1} after 100 cycles at 1 C were obtained for 20-min irradiation at 100% power. As can be seen from TEM images in Figures S1b and S2, the fiber structure was severely damaged after 30-min irradiation at 100% power, resulting in deteriorated conductivity of the EUV-CNF interlayer. The EUV-CNF interlayer suppressed the diffusion of polysulfides became weak when the irradiation time was less than 20 min or the intensity was less than 100% power.

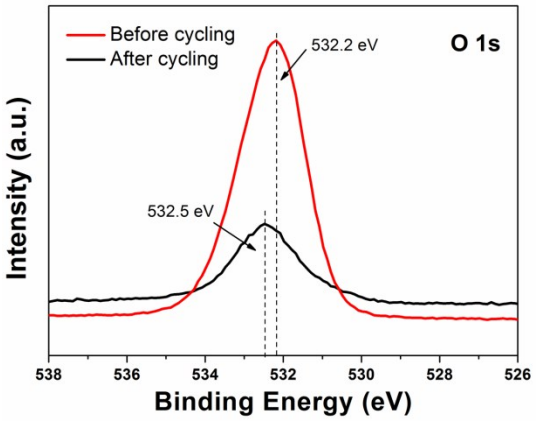

Figure S9 O 1s XPS spectra of the EUV-CNF interlayer before and after cycling.

Table S1 Elemental distributions determined by XPS analysis

Sample	C at%	N at%	O at%	O 1s peak at%			
				OH (533.5 eV)	C–O (532.9 eV)	C=O (531.2 eV)	CO(O) (531.2 eV)
CNF interlayer	86.07	8.66	5.47	1.20	1.47	1.38	1.43
EUV-CNF interlayer	77.63	8.76	13.61	2.40	4.64	3.88	2.69

Table S2 Comparison of processing conditions and electrochemical performances of Li–S batteries with different interlayers

Interlayer type	Functional group	Processing condition	S content in electrode (wt.%)	Cycle number	Capacity retention (mAh g^{-1})	Fading rate (per cycle)	Ref.
MWCNT paper	none	CVD	-	100	855 (0.5 C)	0.41%	3
ZnO/C interlayer	ZnO	300 °C, 3 times; 95 °C, 24 h,	49%	200	776 (1 C)	0.05%	4
CP@CNF	C=N	300 °C, 10 h	60%	200	710 (0.3 C)	0.127%	5
Fe_3C/carbon	C–Fe, C–N	Iron (III) acetylacetonate	70%	100	893 (0.12 C)	0.24%	6
Treated carbon paper	–OH	NaOH/alcohol, 24 h	60%	50	900 (0.2 C)	0.9%	7
PAA-SWNT film	–COOH	PAA	65%	200	573 (1 C)	0.12%	8
TiO_2-CNF	–Ti	600 °C, 2 h	60%	500	520 (0.2 C)	0.121%	9
GO/CNT	C–OH	H_2O_2	70%	200	846 (0.18 C)	0.4%	10
N-rich porous carbon	–N,	Resorcinol, formaldehyde, 70 °C	70%	100	1040 (0.2 C)	0.238%	11
NCF-CNT	–N	-	70%	100	903 (0.5 C)	0.011%	12
RGO/AC	-	H_2SO_4/HNO_3 (3:1) sodium ascorbate	80%	100	665 (0.1 C)	0.38%	13
GO/Nafion	$–SO_3^-–$	Nafion	54%	200	~750 (0.5C)	0.18%	14
EUV-CNF	C=O, –OH	Room temperature, 20 min	70%	200	916 (0.2 C)	0.16%	This work

Table S3 Sulfur content of both sides of CNF and EUV-CNF interlayers

Sulfur content (at %)	CNF interlayer	EUV-CNF interlayer
Sulfur cathode side	7.69	4.59
Separator side	7.17	2.96

References

1. P. Zhu, J. Zhu, J. Zang, C. Chen, Y. Lu, M. Jiang, C. Yan, M. Dirican, R. K. Selvan and X. Zhang, *J. Mater. Chem. A*, 2017, **5**, 15096-15104.

2. J. Zhu, Y. Ge, D. Kim, Y. Lu, C. Chen, M. Jiang and X. Zhang, *Nano Energy*, 2016, **20**, 176-184.

3. Y. S. Su and A. Manthiram, *Chem. Commun.*, 2012, **48**, 8817-8819.

4. T. Zhao, Y. Ye, X. Peng, G. Divitini, H.-K. Kim, C.-Y. Lao, P. R. Coxon, K. Xi, Y. Liu, C. Ducati, R. Chen and R. V. Kumar, *Adv. Funct. Mater.*, 2016, **26**, 8418-8426.

5. Q. Li, M. Liu, X. Qin, J. Wu, W. Han, G. Liang, D. Zhou, Y.-B. He, B. Li and F. Kang, *J. Mater. Chem. A*, 2016, **4**, 12973-12980.

6. J.-Q. Huang, B. Zhang, Z.-L. Xu, S. Abouali, M. Akbari Garakani, J. Huang and J.-K. Kim, *J. Power Sources*, 2015, **285**, 43-50.

7. C. Zu, Y. S. Su, Y. Fu and A. Manthiram, *Phys. Chem. Chem. Phys.*, 2013, **15**, 2291-2297.

8. J. H. Kim, J. Seo, J. Choi, D. Shin, M. Carter, Y. Jeon, C. Wang, L. Hu and U. Paik, *ACS Appl. Mater. Interfaces*, 2016, **8**, 20092-20099.

9. G. Liang, J. Wu, X. Qin, M. Liu, Q. Li, Y. B. He, J. K. Kim, B. Li and F. Kang, *ACS Appl. Mater. Interfaces*, 2016, **8**, 23105-23113.

10. J.-Q. Huang, Z.-L. Xu, S. Abouali, M. Akbari Garakani and J.-K. Kim, *Carbon*, 2016, **99**, 624-632.

11. J. Balach, T. Jaumann, M. Klose, S. Oswald, J. Eckert and L. Giebeler, *J. Power Sources*, 2016, **303**, 317-324.

12. Z. Cao, J. Zhang, Y. Ding, Y. Li, M. Shi, H. Yue, Y. Qiao, Y. Yin and S. Yang, *J. Mater. Chem. A*, 2016, **4**, 8636-8644.

13. H. Li, L. Sun, Y. Zhang, T. Tan, G. Wang and Z. Bakenov, *J. Energy Chem.*, 2017, **26**, 1276-1281.

14. T. Z. Zhuang, J. Q. Huang, H. J. Peng, L. Y. He, X. B. Cheng, C. M. Chen and Q. Zhang, *Small*, 2016, 12, 381-389.